Electronic Supplementary Material (ESI) for Journal of Materials Chemistry A.

Oxygen transport kinetics of the misfit layered oxide $Ca_3Co_4O_{9+\delta}$

V. Thoréton[a], Yang Hu[b], C. Pirovano[a], E. Capoen[a], N. Nuns[a], A.S. Mamede[a], G. Dezanneau[b], C.Y. Yoo[c], H.J.M. Bouwmeester[c], R.N. Vannier[a]*

Electronic Supplementary Information

SIMS analysis

For line-scan[14] analyses, slices of the sample were cut perpendicular to its surface. Two of them were placed side to avoid edge effects of the sample.

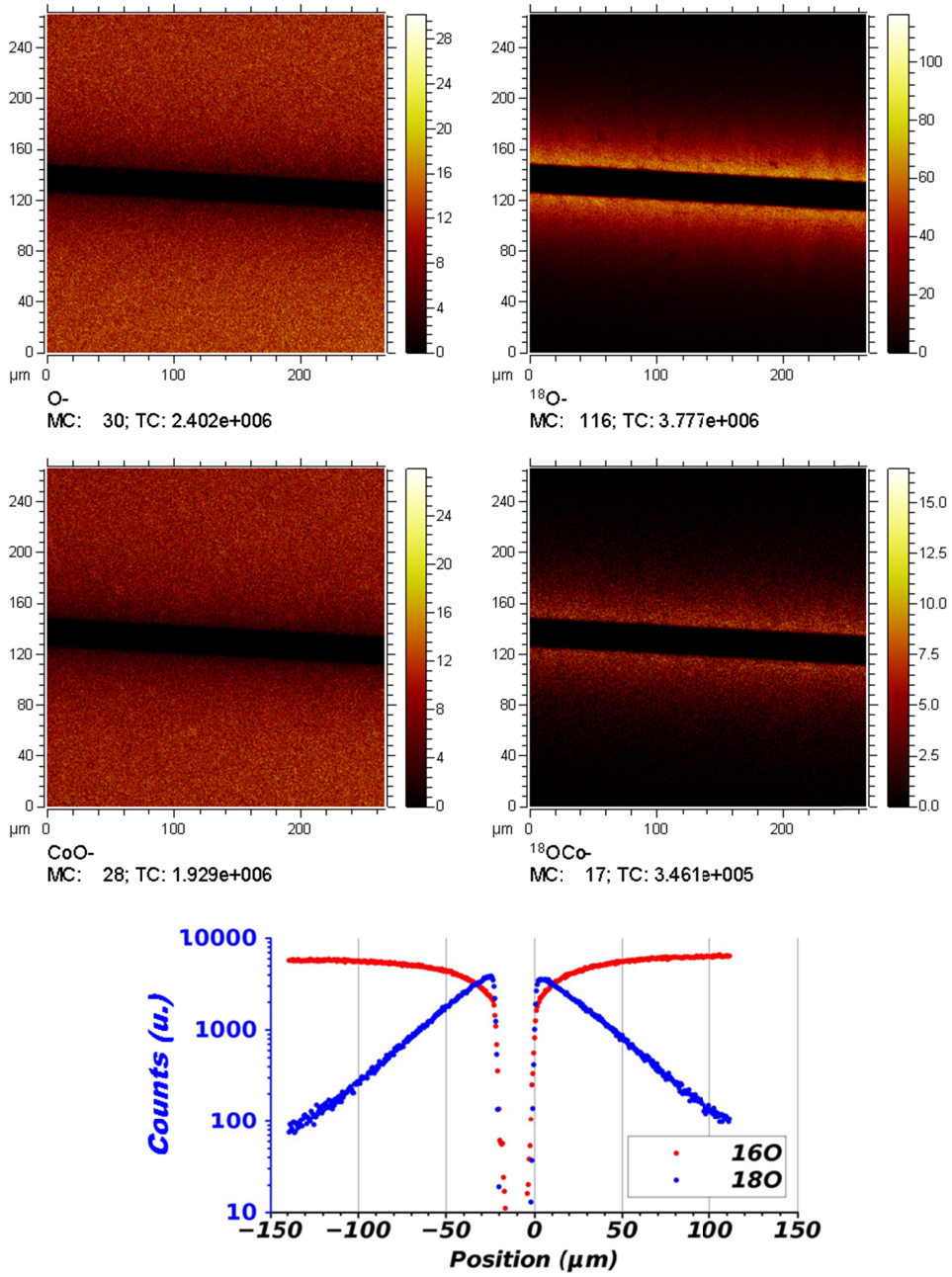

Fig. S1 Ionic cartography of a CCO sample and corresponding line scan.

Depending on the pulse length and intensity of the primary ions, there are different modes of SIMS analysis.[1] The bunch mode uses short pulses (< 0.7 ns) with high intensity (250-1000 ions per pulse), it allows a high mass resolution (Δm/m > 8000) but the spatial resolution is low (2 μm). In case of the burst mode, a long pulse (100 ns) is modulated with a MHz signal in order to cut several 1.5 ns pulses (1 to 10 pulses, bursts) out of a larger ion packet. This mode leads to lower mass resolution (Δm/m = 5000), lower intensity (40 ions per pulse) but to a better spatial resolution (< 350nm) (see Fig. S2).

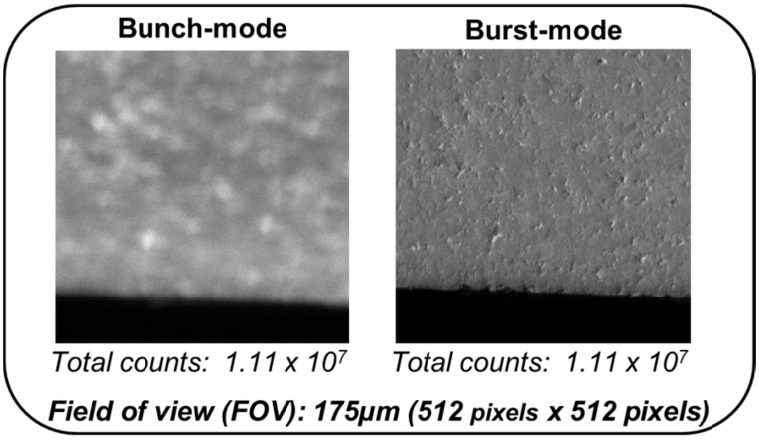

Fig. S2 Cartography of the total ionic signal collected on a slice of CCO pellet, (a) bunch mode, (b) 8 pulses burst mode. The resolution in burst mode is far better since the beam is focussed (scale 175 μm x 175 μm).

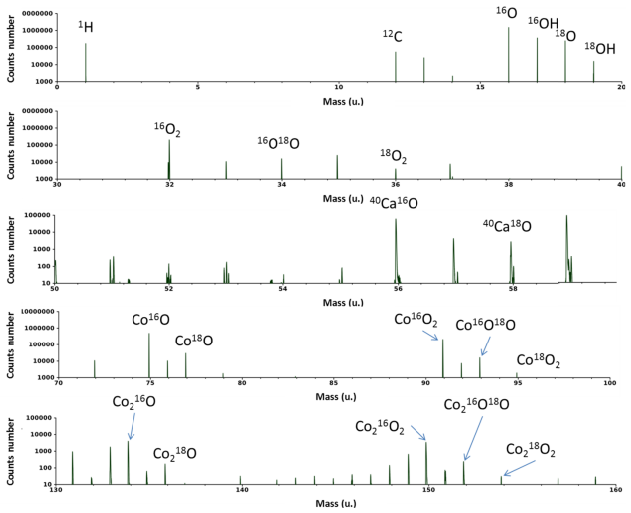

Fig. S3 CCO mass spectra using negative polarity (bunch mode).

A typical mass spectrum collected on a CCO ceramic in bunch mode is given in Fig. S3. Negative secondary ions were chosen because of the high electronic affinity of oxygen. The main species are O_i, Co_nO_x and Ca_mO_y. H is always visible since it is difficult to remove hydrogen contamination in the chamber. OH^- species are due to hydroxides which form at the sample surface by contamination, ^{12}C is also to be noticed. Mass 16 and 18 are the most intense and were used to calculate the isotopic ratio. However, for these masses, one must be careful with saturation. One could also use mass 32 ($^{16}O_2$), 34 ($^{16}O^{18}O$) and 36 ($^{18}O_2$). However, in this case, one

must consider a risk of overlapping with $^{12}C_3$ (35.9983 and 36.0000). Ca exhibits a few isotopes but the relative abundance of 96.94% of ^{40}Ca is high and $^{40}Ca^{16}O$ (56) and $^{40}Ca^{18}O$ (58) could also be used to calculate the isotope fraction. In contrast, cobalt exhibits only one isotope, ^{59}Co. This allows using ^{59}CoO (75 and 77), $^{59}CoO_2$ (91, 93 and 95), $^{59}Co_2O$ (134 and 136) and $^{59}Co_2O_2$ (150, 152 and 154). Therefore, the isotopic profile was also confirmed following ^{16}OCo and ^{18}OCo masses.

Generally a Bi^+ beam was used, however Bi_3^+ and Bi_3^{2+} were also used sometimes as a way to minimise the saturation. In case of too high intensity, the detector may not recover from the high number of secondary ions in the first burst before ions from the second burst arrive. In this case, only the first burst was used in the quantification with Poisson correction on the 1st peak (count per shot < 1) as explained by De Souza in Ref. 1. When no saturation was observed, all the bursts were used.

X-ray diffraction at variable temperatures and controlled atmosheres

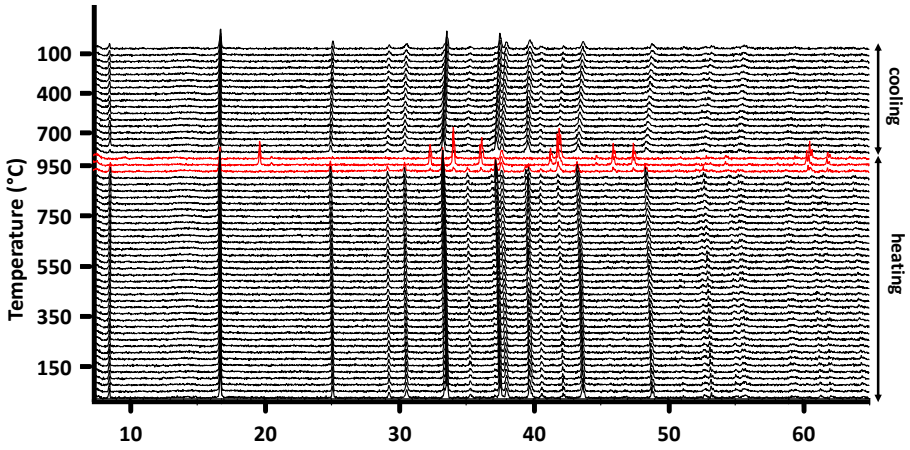

Fig. S4 X-ray diffractograms of CCO at different temperatures. Data acquired from room temperature to 950°C, with 25°C intervals on heating, and 50°C intervals on cooling. The sample decomposes into $Ca_3Co_2O_6$ and CoO at 925°C upon heating, and is transformed back again into CCO at 850°C upon cooling.

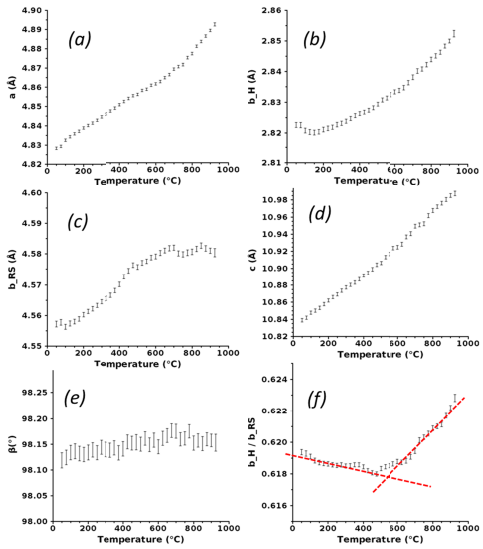

Fig. S5 Temperature dependence of CCO cell parameters. The transition observed at 550°C is confirmed. It is characterised by an increase of the b_{RS}/b_H ratio above this temperature.

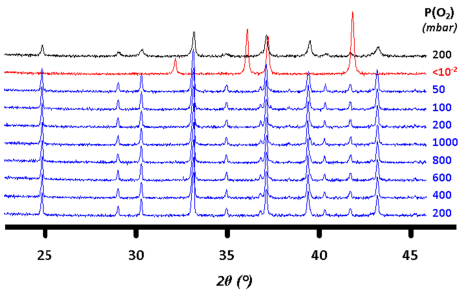

Fig. S6 Stack of CCO X-ray diffractograms at variable oxygen partial pressures at 700°C. CCO is stable from 1 bar to 50 mbar of oxygen, but decomposes under nitrogen atmosphere ($pO2 < 10^{-2}$ mbar) into calcium oxide and cobalt oxide. Interestingly, the phase recombines in less time than it takes to acquire a diffractogram when coming back to 200 mbar of oxygen. It is worth noting that wider Bragg peaks were observed for the diffractogram recorded back to 200 mbar indicating smaller crystallite size.

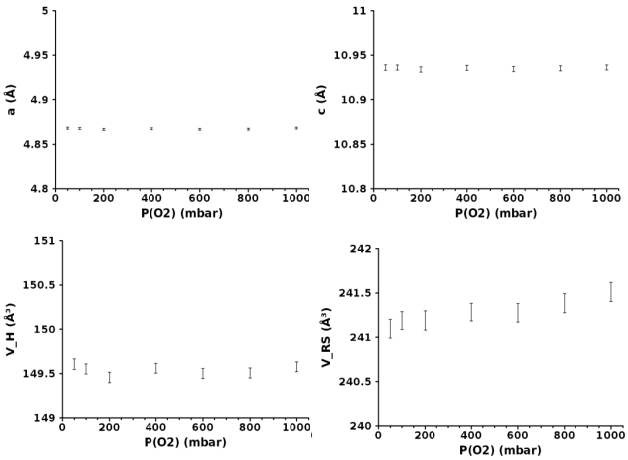

Fig. S7 Evolution of CCO unit-cell parameters in function of the oxygen partial pressure at 700°C. The increase in oxygen partial pressure is mainly characterized by an increase of the volume of the rock salt layers (V_{RS}) when the oxygen partial pressure increased, likely due to a filling of oxygen vacancies in these layers.

TGA analysis at variable temperature and oxygen partial pressure

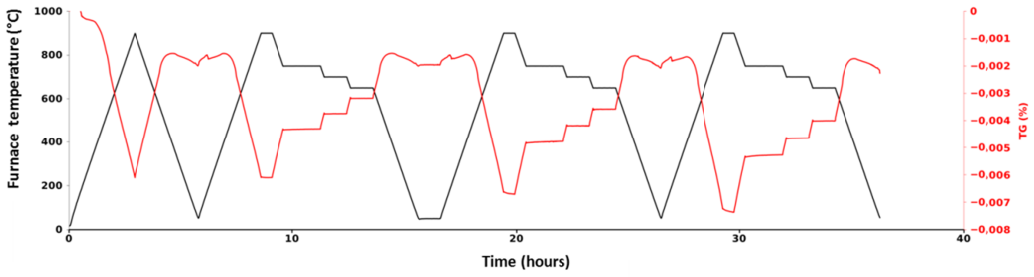

Fig. S8. CCO TGA analysis at variable temperatures and oxygen partial pressures

LEIS on a CCO thin film prepared by Pulse Laser Deposition

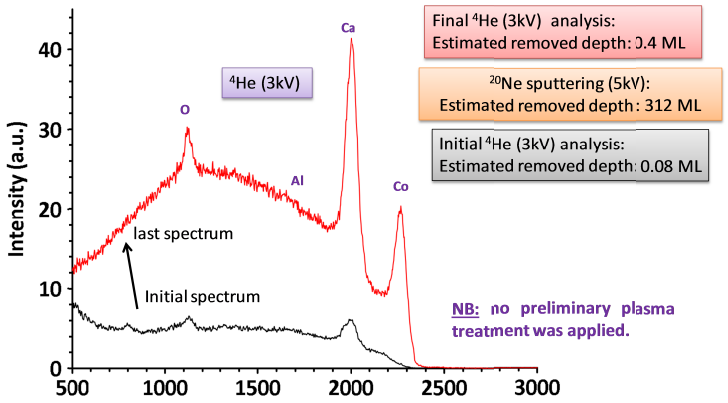

Fig. S9. LEIS analysis carried out on a CCO thin film prepared by Pulse Laser Deposition deposited on a sapphire substrate (Al_2O_3). No trace of sodium was observed.

Table S1. CCO D_{chem} determined by ECR compared to D* measured by IEDP.

Temperature (°C)	D_{chem} air → 0.05 atm D_{chem} 0.05 atm → air	D_{chem} (mean) ($cm^2.s^{-1}$)	$D^*_{ECR}=\frac{D_{chem}}{\gamma}$	D* ($cm^2.s^{-1}$)
650	$3.83.10^{-8}$ $3.89.10^{-8}$	$3.86.10^{-8}$	$1.7.10^{-10}$	$3.0.10^{-10}$
675	$5.45.10^{-8}$ $5.40.10^{-8}$	$5.43.10^{-8}$	$2.4.10^{-10}$	-
700	$9.28.10^{-8}$ $9.06.10^{-8}$	$9.17.10^{-8}$	$4.3.10^{-10}$	$2.7.10^{-10}$
725	$1.11.10^{-7}$ $1.21.10^{-7}$	$1.16.10^{-7}$	$5.6.10^{-10}$	-
750	$1.73.10^{-7}$ $1.61.10^{-7}$	$1.67.10^{-7}$	$8.4.10^{-10}$	$6.5.10^{-10}$

Table S2. CCO surface exchange derived by PIE compared to IEDP.

Temperature/°C	k_s (PIE)/$cm.s^{-1}$	k* (IEDP)/$cm.s^{-1}$
500	$3.68(7).10^{-9}$	-
550	$1.92(4).10^{-8}$	-
600	$1.16(3).10^{-7}$	$4.2.10^{-8}$
650	$2.86(6).10^{-7}$	$8.0.10^{-8}$
700	$7.2(2).10^{-7}$	$1.6.10^{-7}$
750	$1.57(3).10^{-6}$	$5.0.10^{-6}$

References

1. R.A. De Souza, J. Zehnpfenning, M. Martin, J. Maier, *J. Solid State Ionic*, 2005, **176**, 1465.